Direct Current Magnetic Hall Probe Technique for Measurement of Field Penetration in Thin Film Superconductors for Superconducting Radio Frequency Resonators

I. H. Senevirathne,[1,2,a)] A. Gurevich,[1] and J. R. Delayen[1,2]
[1)]*Department of Physics and Center for Accelerator Science, Old Dominion University, Norfolk, VA 23529, USA*
[2)]*Thomas Jefferson National Accelerator Facility, Newport News, VA 23606, USA*

(Dated: 19 April 2022)

Superconducting Radio Frequency (SRF) cavities used in particle accelerators are typically formed from or coated with superconducting materials. Currently high purity niobium is the material of choice for SRF cavities which have been optimized to operate near their theoretical field limits. This brings about the need for significant R&D efforts to develop next generation superconducting materials which could outperform Nb and keep up with the demands of new accelerator facilities. To achieve high quality factors and accelerating gradients, the cavity material should be able to remain in the superconducting Meissner state under high RF magnetic field without penetration of quantized magnetic vortices through the cavity wall. Therefore, the magnetic field at which vortices penetrate in a superconductor is one of the key parameters of merit of SRF cavities. Techniques to measure the onset of magnetic field penetration on thin film samples need to be developed to mitigate the issues with the conventional magnetometry measurements which are strongly influenced by the film orientation and shape and edge effects. In this work we report the development of an experimental setup to measure the field of full flux penetration through films and multi-layered superconductors. Our system combines a small superconducting solenoid which can generate the magnetic field up to 500 mT at the sample surface and three Hall probes to detect the full flux penetration through the superconductor. This setup can be used to study alternative materials which could potentially outperform niobium, as well as SIS multilayer coatings on niobium.

I. INTRODUCTION

Strong radio-frequency electromagnetic fields generated in superconducting linear particle accelerator propel a beam of charged particles such as protons or electrons to very high energies. The maximum accelerating field which superconducting radio-frequency (SRF) resonator cavities can withstand is one of the key parameters of merit of particle accelerators. Currently, the material of choice for the best SRF cavities is niobium (Nb), because it has a relatively high critical temperature T_c and the highest lower critical magnetic field B_{c1} among all superconductors. In addition, niobium is chemically inert, widely available and very suitable for machining and deep drawing[1]. However, the large number of Nb cavities in a big accelerator operating at the superfluid helium temperature below 2K require costly cryogenic equipment and a significant RF input power. Performance of Nb cavities can be limited by multipacting, trapped magnetic flux, field emission and thermal breakdown which mostly result from topographic surface imperfections and nonsuperconducting materials precipitates[1]. Recent technological advances have significantly mitigated these issues and increased the accelerating gradients from a few MV/m to $45-50$ MV/m[2–6]. As a result, the best Nb cavities can now operate at RF field amplitudes close to a theoretical limit at which the surface RF magnetic field approaches the superheatihg field B_{sh}[7–9]. Further progress in the SRF accelerator technology demands even higher accelerating gradients and lower RF losses, while increasing the operating temperature to 4.2 K or higher. This challenging task can only be accomplished using superconductors which have higher critical temperatures than $T_c = 9.2$ K of Nb.

Besides a higher T_c another important parameter of merit of the SRF cavity material is the field onset of penetration of quantized magnetic vortices which cause strong dissipation under RF field. In a type -II superconductors vortices become energetically favorable at dc fields exceeding the lower critical field B_{c1}. However, because of the Bean-Livingston magnetic surface barrier for penetration of vortices, the low-dissipative Meissner state can remain metastable at higher fields $B_{c1} < B < B_{sh}$. Here B_{sh} is a superheating field at which the Bean-Livingston barrier disappears and the Meissner state becomes unstable. The superheating magnetic field thus defines a theoretical field limit of SRF breakdown at which explosive flux penetration accompanied by high RF losses occurs[10,11]. Currently the best Nb cavities can operate at the peak magnetic field around 200-220 mT, which is close to B_{sh} for Nb[1].

Properties of some alternative SRF materials in comparison to Nb are shown in Table 1. Even though these superconductors have higher T_c and B_{sh}, all of them have B_{c1} lower than that of Nb. Smaller B_{c1} make alternative superconductors prone to premature flux penetration and high RF losses at fields well below B_{sh}. This is because materials or topographic defects on the cavity surface reduce the Bean-Livingston barrier, causing local flux penetration at $B_{c1} < B_p < B_{sh}$ or even at $B_p < B_{c1}$ for polycrystalline superconductors with weakly-coupled grain boundaries[12], which is particularly relevant for Nb_3Sn or superconducting pnictides[13]. To address the problem of premature flux penetration in low-B_{c1} superconductors, a SIS multilayer coating has been proposed[14,15]. In this case the inner surface of the Nb cavity is coated with thin su-

[a)]Electronic mail: isene001@odu.edu

TABLE I. Superconducting properties of some alternative superconductors for SRF applications.

Material	T_c (K)	B_c (mT)	B_{c1} (mT)	λ (nm)
Nb	9.2	200	170	40
NbN	16.2	230	20	200
Nb_3Sn	18	540	40	85
MgB_2	40	320	20-60	140
$B_{0.6}K_{0.4}BiO_3$	31	440	30	160

perconducting (S) layers having higher T_c and B_{sh} separated by thin insulating (I) layers, as depicted in Fig. 1. Here S layers should be thinner than the London penetration depth λ_L of the superconductor. The increase of the parallel B_{c1} in thin films and SIS structures has been tested on Nb_3Sn[16], MgB_2[17], NbN[18,19] and NbTiN[20]. For I interlayers which suppress Josephson coupling[21] SiO_2[18], MgO[19] and AlN[20] have been used.

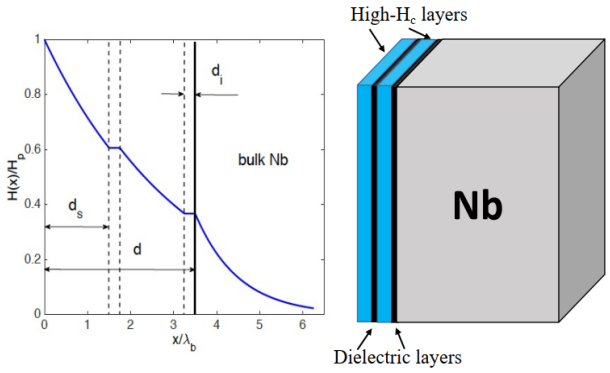

FIG. 1. Multilayer system comprised of alternative S layers with thickness $< \lambda_L$ and thin I layers deposited on the inner surface of the Nb cavity (right). Distribution of the magnetic field in a multilayer of thickness d. Dashed lines show boundaries between dielectric and superconducting layers (left).

The onset of magnetic field penetration B_p in thin film of SIS multilayer structures is an important characteristic of high-field performance of alternative materials for SRF cavities[21] but the measurements of B_p on thin film test samples under the conditions emulating those of SRF cavities are challenging. The problem is that the RF magnetic field in the accelerating TM mode in the cavity is parallel to the surface of the superconductor so the screening Meissner RF currents only flow in a thin layer $\sim \lambda_L$ at the inner surface of the cavity. However, in typical dc magnetometry measurements, B_p is extracted from the field dependence of the magnetic moment, $M(B)$ of a sample placed in a nearly uniform magnetic field. In this case the magnetic field is applied to both sides of the sample, and $M(B)$ depends strongly on the geometry of a flat sample and its orientation with respect to B[22]. The so-obtained values of B_p are strongly influenced by pinning of vortices and surface and magnetic geometrical barriers[23,24] and thus are hardly representative of B_p for the SRF cavity geometry.

Several methods have been developed to measure the field-dependent quality factors $Q(B)$ and the breakdown fields on test thin film samples of alternative SRF materials. In a quadrupole resonator technique a thin film sample deposited onto a 3" substrate is welded to the niobium resonator[25,26]. However, this technique can only probe a low-field part of $Q(B)$ (currently up to 60 mT well below $B_{sh} \approx 240$ mT of Nb) and cannot measure the breakdown fields $\simeq B_{sh}$ of the promising SRF materials as all of them have B_{sh} higher than B_{sh} of Nb. A way around this problem is to measure the flux penetration field for a thin film sample placed in a parallel dc magnetic fields of superconducting solenoids which can produce fields well above B_{sh}. This was implemented in Ref. 27 in which the Hall probes were used to detect the penetration field of thin films deposited onto a stainless steel hollow tube. This technique allows one to apply a strong dc magnetic field parallel to the outer surface of the superconducting film but requires uniform film coating of a long cylindrical tube and cannot be used to measure test thin film of multilayer small flat samples of different SRF materials.

The problems outlined above bring about the need to develop a simple technique to measure the flux penetration field through thin film or SIS multilayer sample typically deposited onto 1-2" substrates. This technique should provide a parallel magnetic field applied to only one side of the sample to emulate the field configuration of SRF cavities. In this work we report the development of such a technique which includes a Hall probe experimental setup for the measurement of the field of full flux penetration B_p through a flat superconducting sample placed under a small superconducting solenoid which can generate magnetic field higher than 500 mT. To illustrate the capabilities of this setup, we also present preliminary results of measurements of B_p on bulk Pb and Nb, Nb_3Sn thin film and Nb_3Sn/Al_2O_3 multilayer samples.

II. MEASUREMENT TECHNIQUE

We developed a setup to measure the field of full flux penetration using the approach similar to a two-coil technique which has been widely used for the measurements of the magnetic penetration depths and coherence lengths in superconducting films[28–33]. The schematics of our setup is shown in FIG.2.

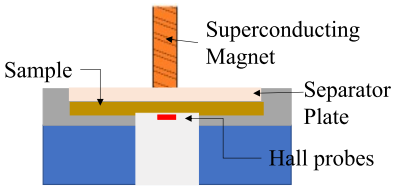

FIG. 2. Main features of experimental setup. A superconducting solenoid is placed above the sample top surface to apply a magnetic filed. Hall probes are mounted at the bottom of the sample to detect magnetic filed penetrated through the sample. A separator plate provides a fixed gap between the magnet and the sample.

A group from Daresbury Laboratory used a ferrite C-

shaped dipole magnet along with a superconducting solenoid to generate a parallel magnetic field at the surface of a flat sample. In their setup one Hall probe was used to read the applied field and the other one to detect the field penetrating through the sample[34]. Our experimental setup depicted in Fig. 2 uses a similar approach but is able to generate high surface magnetic field without the use of ferrite. Here a superconducting solenoid is placed above the sample to apply dc magnetic field to one surface of the film. Instead of using a Hall probe to read the applied magnetic field on the sample surface, we calibrated the applied magnetic field generated at different magnet currents, which helps to minimize the separation between magnet and the sample and hence to achieve magnetic field high enough to test various superconducting samples having higher superheating field, H_{sh}. Three magnetic Hall sensors are mounted under the sample to detect penetrated magnetic field through the sample. A 0.5 mm thick separator plate made of sapphire (Al_2O_3) is inserted between the sample and the magnet to maintain a fixed separation between them and protect the sample during the experiment. This setup can house flat samples up to 50 mm in diameter and thicknesses up to a few millimeters. The assembled setup is submerged in liquid helium bath which allows us to investigate the magnetic flux penetration at the temperatures such as 4.35 K and 2 K.

In the course of the measurements a sample is cooled down to either 4.35 K or 2 K at zero magnetic field and then the magnet current is increased gradually to apply a magnetic field. If a superconductor thicker than a few λ_L is in the Meissner state, it screens the external magnetic field so no magnetic field is detected by the Hall probes mounted on the other side of the sample. Once the external field exceeds B_p, vortices enter the superconductor and the magnetic flux breaking through the sample is detected by the magnetic sensors.

A. Magnet Design

The superconducting magnet was fabricated by winding a NbTi thin wire on a dielectric spool using a lathe machine. This magnet has 4 layers of homogeneous wingdings with 78 turns per each layer. An epoxy was used to insulate the layers and provide a monolithic structure which does not allow movement of the wire inside the coil. This NbTi wire of diameter 0.325 mm can carry a maximum current up to 100 A. The assembled magnet has a bore diameter of 8.93 mm and length 25.35 mm and can generate the magnetic field greater than 500 mT.

The expected field distribution around our magnet placed above the superconducting sample was simulated using the Poisson computer code. The results shown in FIG.3 were obtained for the parameters of our coil, a fixed 1 mm gap between the magnet and the sample and 100 A of magnet current. The diameter of our magnet was chosen to be five times smaller than the sample diameter of 50 mm to avoid penetration of magnetic field at the film edges.

FIG 3 shows that a thick superconducting sample in the Meissner state acts as a magnetic mirror, which can be modeled by adding an image magnet placed on the other side of the sample. As a result, the vertical component of the magnetic field (B_z) cancels out and the radial field component parallel to the film surface is twice the radial magnetic field (B_r) produced by the solenoid in free space. This field configuration caused by screening current flowing at the top surface of the sample mimics the field distribution in SRF cavities. If a sample is thinner than a few λ_L the applied magnetic field is partially screened, and the z-component of this field is detected by the Hall probes attached at the bottom of the sample. Once the applied parallel field exceeds a critical value at which vortex semiloops start penetrating the film and reaching its opposite side, the Hall probe detects a jump-wise increase in B_z. In the case of thick films with $d \gg \lambda_L$ studied in this work, the Hall probes detect no signal as long as the magnetic flux does not break through the sample. However, once the magnetic field breaks through the sample, the Hall probe detects the vertical component B_z produced by penetrating vortices, which allows us to measure the field of full flux penetration and the critical magnetic fields of the superconductor, as described below.

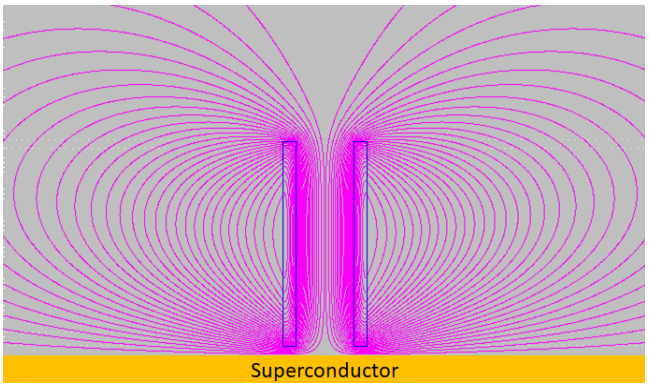

FIG. 3. The calculated magnetic field around the multi turn coil is expelled from the interior of the superconductor in the Meissner state, which makes the filed lines parallel to the sample surface and mimic the field configuration at the inner cavity surface.

B. Magnetic Sensors

The onset of the magnetic field penetration through the sample is measured by three Hall sensors mounted underneath the sample. The Hall probes were calibrated by passing a few tens of mAs through the probe and by measuring the Hall voltage U_H proportional to the applied magnetic filed, as shown in FIG. 4(a). In our setup we used HHP-NP Hall probes from Arepoc to measure the magnetic field normal to the sensor. These HHP-NP probes have sensitivity of 70 mV/T and can operate at temperatures between 1.5 K and 350 K in a magnetic fields up to 5 T.

The active area center is marked by a cross located on the top surface of the sensor package with accuracy better than ± 0.1 mm. The dimensions of the active area are $500 \times 100\,\mu$m, and the overall dimensions are $7 \times 5 \times 1$ mm. The model HHP-NP is a probe covered by a synthetic resin

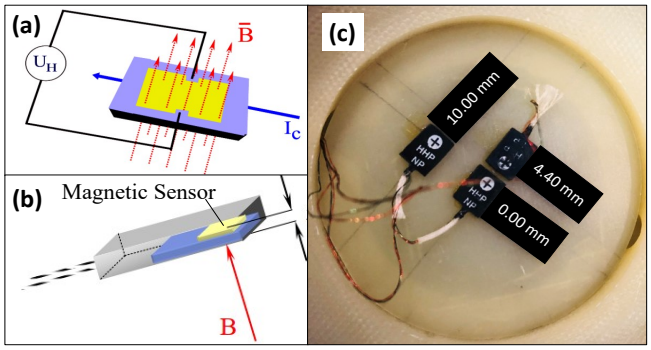

FIG. 4. (a) HHP-NP Hall probes used in the experimental setup which can detect the component of the magnetic field perpendicular to probe (b) the Hall sensor located inside the probe covered with the resin (c) configuration of the Hall probes mounted at the bottom of the sample.

in transverse modification and the electrical system is parallel to the bottom surface with high accuracy (FIG. 4(b)). In our setup, three Hall probes are mounted under the sample, one is at the center other two are at 4.40 mm and 10.00 mm from the center as shown in FIG. 4(c) in order to study the penetrated field profile along the sample radius.

All components of the setup were assembled in a nonmagnetic container, as shown in FIG.5. The superconducting wires in the magnet were connected to copper current leads which can carry up to 80-90 A. Other features of the setup are: finger springs which push the magnet down to avoid vertical movement of the assembly, G10 plate to permanently mount the Hall probes, and a separator plate between the magnet and the sample to maintain a fixed gap between them and protect the sample surface. According to our simulations, if the gap between the magnet and the sample varies by 0.1 mm, the maximum surface magnetic field changes nearly by 7%. Furthermore, measurements of flux penetration on thin films are sensitive to surface or edge defects which can cause premature local penetration of vortices. In turn, the heat generated by penetrating vortices causes more vortices to enter the sample which produces more heat and eventually a thermomagnetic avalanche[35,36]. Such partial local flux jumps are particularly pronounced at low temperatures as the specific heat $C(T) \propto T^3$ decreases with T. To mitigate the flux jumps, the sapphire separator plate was replaced by a copper plate to improve heat transfer from the sample to He bath[37].

III. CALIBRATION

Setup calibration was performed in several steps to find the maximum magnetic field from the magnet at the sample surface. First, two separate measurements were done without the sample. As shown in FIG. 6, these two tests were done under the same conditions but with different vertical spacings between the magnet and the magnetic sensor. In test 01, top surface and in test 02 bottom surface of the Hall probe is closer to the magnet.

In both tests, the vertical components of the magnetic field (B_z) at the positions of all three Hall probes were recorded as functions of the magnet current. Measurements were performed both in increasing and decreasing fields to test the linearity of the characteristic curves shown in FIG.7. With the dipole-like magnetic field distribution of the solenoid, the vertical magnetic field component decreases rapidly within the lateral distance from the magnet axis.

The characteristic Hall probe curves inferred from both tests were used to calculate the vertical magnetic component at three different probe locations which would be observed at 100 A of the magnet current. At the same time, the vertical magnetic field along the sample radius was simulated for 100 A of magnet current. FIG.8 compares the observed magnetic filed detected by the Hall probes with the simulated magnetic field for 100 A. A difference between the measured (black dots) and simulated fields (dashed curves) is mainly due to an uncertainty in the spacing between the Hall probes and the magnet. When we corrected the spacing by 0.19 mm (less than the thickness of NbTi wire), the experimental magnetic fields coinside with the simulations.

Finally, simulation was ran to find the maximum magnetic field at the sample surface with the magnet current of 100 A taking into account the spacing correction of 0.19 mm mentioned above. The so-obtained radial field distribution $B_\parallel(r)$ shown in FIG.9 is similar to the field between two antiparallel magnetic dipoles spaced by $2d$ with the peak in the radial field $B_\parallel(r)$ at the distance $r \sim 4d$ from the magnet axis. The calculated maximum surface magnetic field 6.26 mT/A was used to calculate maximum $B_\parallel(r)$ at different magnet current. This applied surface magnetic field is independent of the sample thickness if the sample is thicker than the London penetration depth. From $B_\parallel(r)$ we readily infer the radial distribution of the screening supercurrent density in a thick film: $J_\parallel(r,z) = (B_\parallel(r)/\mu_0)e^{-z/\lambda_L}$, where $z = 0$ corresponds to the surface of the superconductor. Once the maximum screening current density along the ring of radius $\approx$ 4mm where $B_\parallel(r,0)$ is maximum exceeds the depairing current density $J_d = H_{sh}/\lambda_L$ the Meissner state becomes unstable with respect to penetration of vortices. This measurement setup was tested on bulk Nb and Pb superconductors, as described below.

IV. MEASUREMENTS OF B_p IN LEAD AND NIOBIUM

Our setup was tested on lead (type I superconductor) and niobium (marginal type II superconductor). FIG.10 shows the observed magnetic field signal at three Hall probes as a function of the maximum surface magnetic field for lead (a) and niobium (b) 250 μm thick samples at 4.35 K. Concurrent first flux penetration through the sample was detected by all three Hall probes, the center probe detected the strongest penetrated magnetic field. Side Hall probes from the center detected weaker field and the field of opposite polarity at 10.00 mm in niobium sample. These measurements show at $B > B_p$ a central circular region of the sample is in a field transparent mixed state while the peripheral parts of the sample remain in the Meissner state. The opposite field polarity detected by

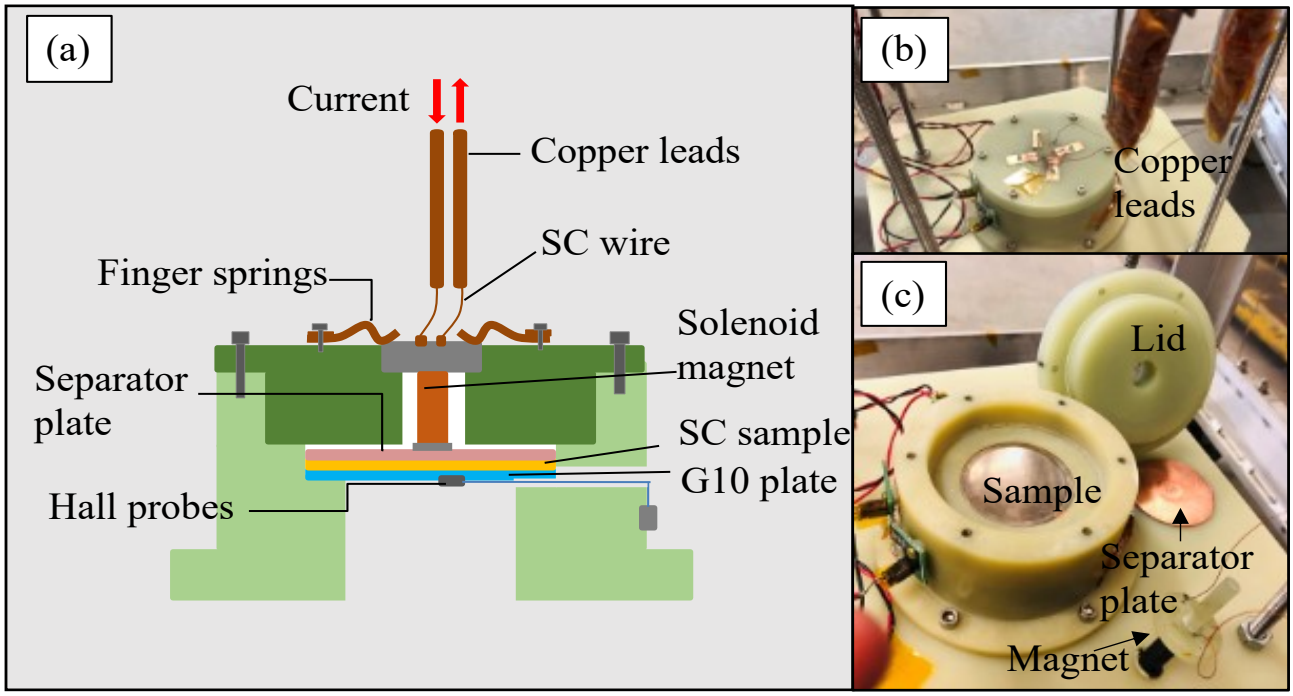

FIG. 5. The nonmagnetic container supports magnetic coil, sample and magnetic sensors symmetrically (a) cross sectional (b) outer (c) inner view of the non magnetic container. Two copper leads are connected to the magnet to pass high current. This setup is assembled in a cryogenic insert at Jefferson Lab to perform the experiment at cryogenic temperatures.

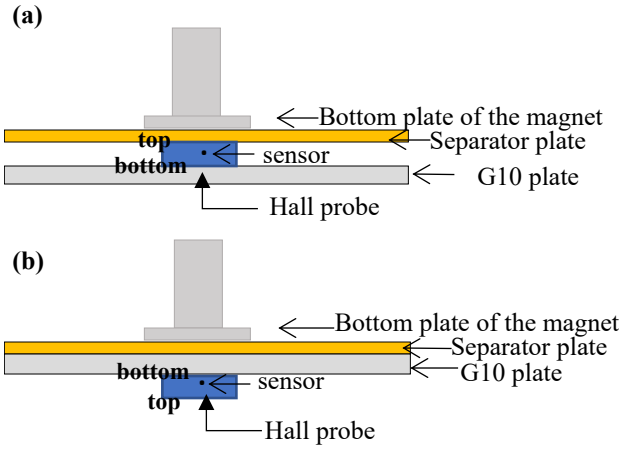

FIG. 6. Setup arrangement with the orientation of Hall probes for the calibration (a) Test 01: Hall probes are upside and (b) Test 02: Hall probes are downside.

the Hall probe at 10 mm in Nb is consistent with the dipolar return field of the magnet focused in a circular region of the mixed superconducting state.

It turns out that the measured field onset of full flux penetration in thick samples with $d \gg \lambda_L$ depends on the film thickness d. The results for lead samples of four different thicknesses at 4.35 K are shown in FIG. 11(a). Here all three Hall probes detected the first penetrated flux simultaneously. The experiments showed that the maximum surface magnetic field $B_p(d)$ at which the magnetic flux breaks through the sample is a linear function of the sample thickness d. Extrapolation of $B_p(d)$ to thickness $\sim \lambda_L$ gives $B_p(0) = 51.73$ mT, close to the thermodynamic critical field of clean lead, $B_c = 52.64$ mT at 4.35 K[38].

We performed the same measurements on niobium samples of different thicknesses at 4.35 K and 2.00 K in which case all three Hall probes also detected a nearly simultaneous flux penetration. The resulting full flux penetration field $B_p(d)$ also exhibits a linear dependence on the sample thickness, as shown in FIG. 11(b). Extrapolations of $B_p(d)$ to $d \gtrsim \lambda_L$ give $B_p(0) = 132.54$ mT at 4.35 K and $B_p(0) = 163.30$ mT at 2.00 K. It turned out that these values of B_p agreed well with the temperature-dependent lower critical field $B_{c1}(T)$ of clean niobium which can be described by a conventional formula,

$$B_{c1}(T) = B_{c1}(0)[1 - (T/T_c)^2], \quad (1)$$

where $T_c = 9.25$ K and $B_{c1}(0) \simeq 173.5$ mT[39]. From Eq. (1) we get $B_{c1} = 135.1$ mT at 4.35 K and $B_{c1} = 165.4$ mT at 2.00 K. The slightly lower observed values of $B_p < B_{c1}$ may be attributed to the reduction of B_{c1} by nonmagnetic impurities[10,11] in our samples.

The thickness dependence of $B_p(d)$ at $d \gg \lambda_L$ results from penetration of vortex semi-loops from the side of the sample exposed to the field of the magnet. As the surface field increases, the size and the number of vortex semi-loops gradually increase until they reach the opposite side of the sample where they produce perpendicular field components detected by the Hall sensors, once the applied surface field reaches the field of full flux penetration B_p. This field at which the vortex semi-loops reach the opposite side of the

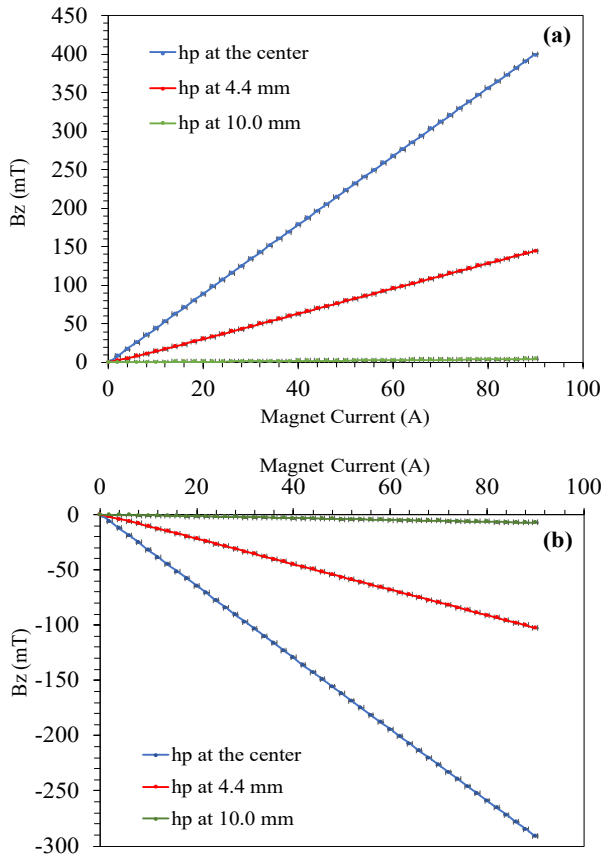

FIG. 7. Vertical component of the magnetic field against magnet current at three Hall probe (hp) positions in (a) Test 01 (b) Test 02.

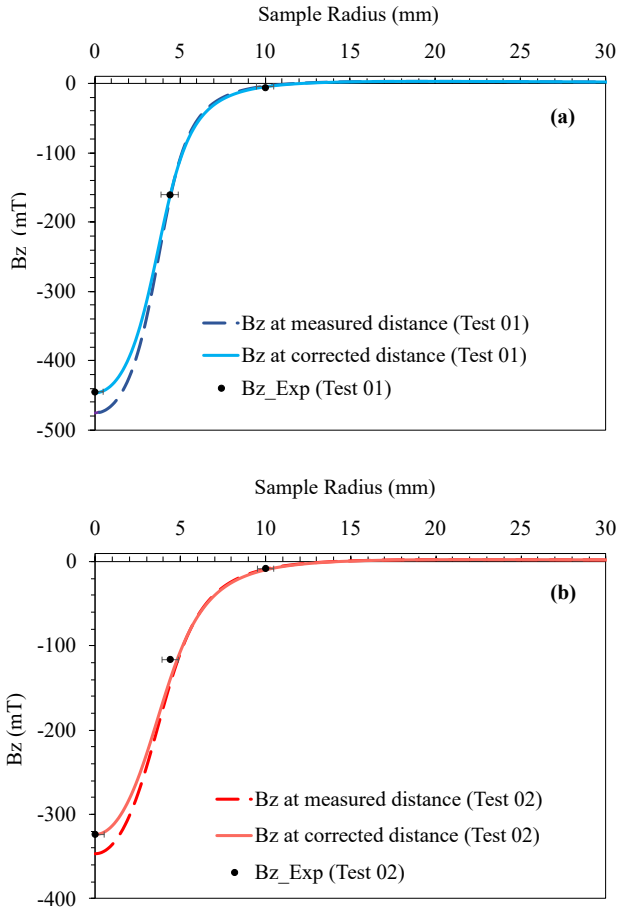

FIG. 8. The simulated vertical component of the magnetic field profile along the sample radius at measured distance (dashed line) and corrected distance (solid line) from magnet to the sensor for 100 A. Extrapolated magnetic field from experimental curves in FIG.7 at three Hall probe positions for 100 A are marked by black dots. (a) test 01 (b) test 02.

sample increases with the thickness of the sample. In this quasi-macroscopic limit, the observed linear thickness dependence of $B_p(d)$ is qualitatively consistent with the Bean critical state model in which the flux density profile in the superconductor changes linearly with the distance z from the surface $B(z) = B_{\parallel} - B_p(0) - \mu_0 J_c z$. Here $B_{\parallel}$ is the applied field which varies along the surface over radial distances much larger than d, $B_p(0) \approx B_{c1}$ is a jump in $B(z)$ in the surface layer of thickness $\simeq \lambda$ due to the Meissner current and equilibrium magnetization of vortices [40], and the depinning critical current density J_c is assumed independent of B at $B \ll B_{c2}$[11]. Hence, the surface field $B_p(d)$ at which the flux reaches the opposite side of the sample takes the form:

$$B_p(d) = B_p(0) + \mu_0 J_c d. \qquad (2)$$

From Eq. (2) and the slope of $B_p(d)$ for Nb at 4 K shown in FIG 11b, we get the critical current density $J_c = [B_p(d_m) - B_p(0)]/\mu_0 d_m \approx 1.4 \times 10^8$ A m^{-2} consistent with J_c values for the cavity-grade Nb with weak flux pinning[41]. Here $B_p(0) =$ 132.5 mT and $B_p(d_m) = 310$ mT at $d_m = 1$ mm were taken from FIG 11b. Although pinning of vortices by the material defects affects the measured $B_p(d)$, the extrapolation of $B_p(d)$ to $d \simeq \lambda_L \lesssim 0.1\,\mu$m much smaller than thicknesses $0.1 - 1$ mm of our samples may give either a bulk critical magnetic field B_c for a type-I superconductor (Pb) or the lower critical field B_{c1} in a type-II superconductor (Nb). As shown above, this procedure yields the extrapolated values of B_p close to the known values of B_{c1} and B_c for Nb and Pb. The nearly linear dependence of $B_p(d)$ also indicates that pinning of vortices and J_c in our samples are not significantly affected by the film thickness.

In SIS multilayers the dielectric I-layers are very effective planar pinning centers which block the expansion of vortex semi-loops to the bulk [15]. In the case of an ideal surface and S-I interfaces, the vortex semi-loops can break through the I-layers if the surface field becomes close to the superheating field $B_{sh} \gg B_{c1}$. In a more realistic situation B_{sh} can be locally reduced by surface materials defects, yet the measurements of B_p allows us to directly observe the enhancement of the magnetic breakdown field by a multilayer as compared to a bare film coating of the same thickness. Here the full flux

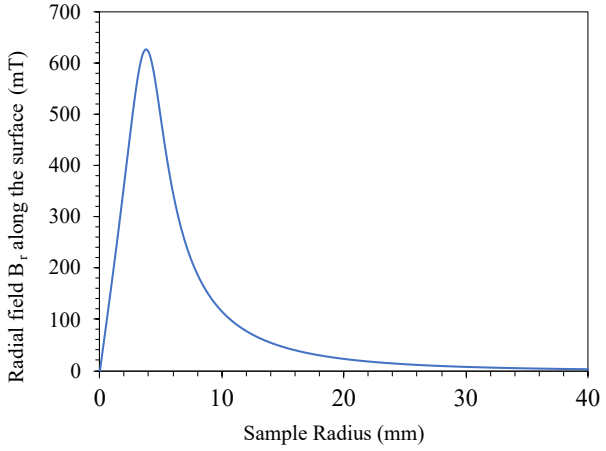

FIG. 9. Radial field B_r on the surface of an ideal superconductor in the Meissner state at 100 A is corrected using above steps and maximum magnetic field is 6.26 mT/A. B_z in the Meissner state is zero.

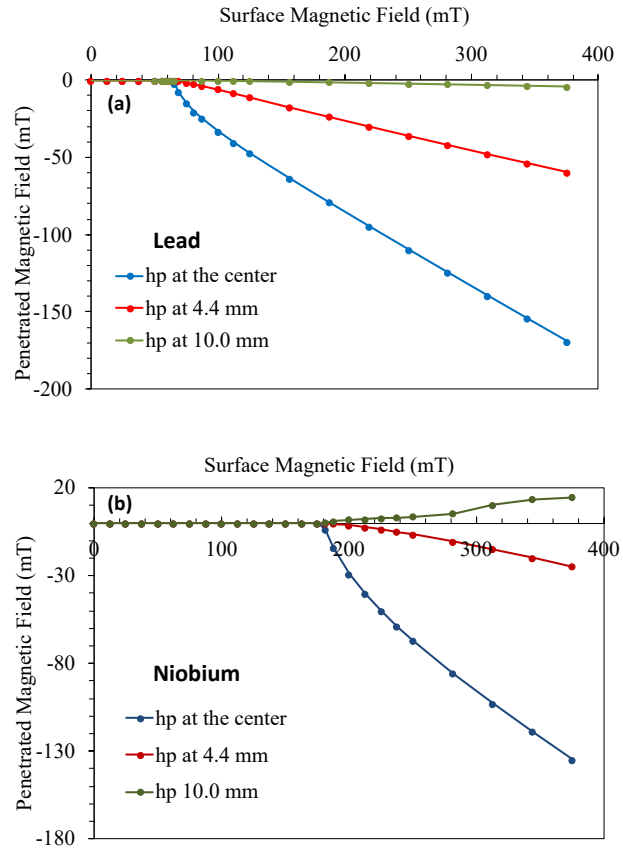

FIG. 10. Penetrated magnetic field detected from three Hall probes (hps) through 250 μm thick (a) lead and (b) niobium samples when the surface magnetic field is increased gradually at 4.35 K.

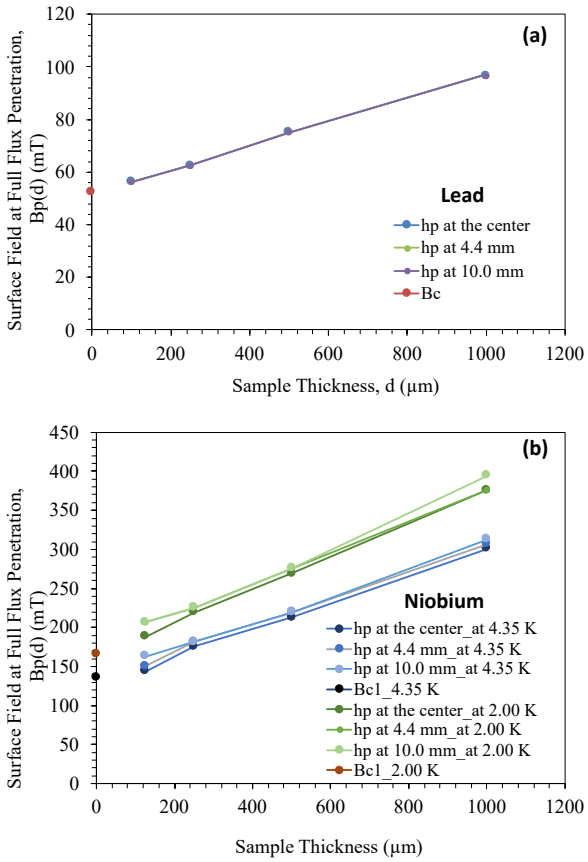

FIG. 11. The surface magnetic field of full flux penetration through the sample, $B_p(d)$ at three Hall probe (hp) locations as a function of sample thickness for: (a) lead at 4.35 K and (b) niobium at 4.35 K and 2.00 K. Here $B_p(d)$ extrapolated to zero thickness is close to B_c of lead at 4.35 K [38] and B_{c1} of niobium at 4.35 K and 2.00 K [39].

penetration field quantifies the field magnitude by which the bulk of the Nb cavity is screened by a multilayer.

Our setup was used to measure B_p in Nb_3Sn films and multilayers. The Nb_3Sn thin film was grown on Al_2O_3 wafer by multilayer sequential sputtering at room temperature and annealed at 950 ^oC by Nizam Sayeed at Jefferson Lab[42] and Nb_3Sn/Al_2O_3 multilayer was grown on Al_2O_3 wafer by high-temperature confocal sputtering by Chris Sundahl at University of Wisconsin-Madison. This multilayer contained four 125 nm Nb_3Sn layers separated by 6 nm Al_2O_3 interlayers, and a 200 nm thick Nb film was deposited on the back side of the Al_2O_3 wafer to prevent leakage of RF field during cavity measurements[16]. We found that the measured flux penetration field can depend on the magnetic field ramp rate and the efficiency of heat transfer from the samples. For instance, at the magnetic field ramp rate 3.13 mT/s (current ramp rate of 0.5 A/s) we observed a sequence of jumpwise penetrations of magnetic flux shown by the blue curves in FIG.12. This behavior is indicative of partial thermomagnetic flux jumps caused by the positive feedback of the heat generated by moving vortices and the number of penetrating vortices [35,36]. Here

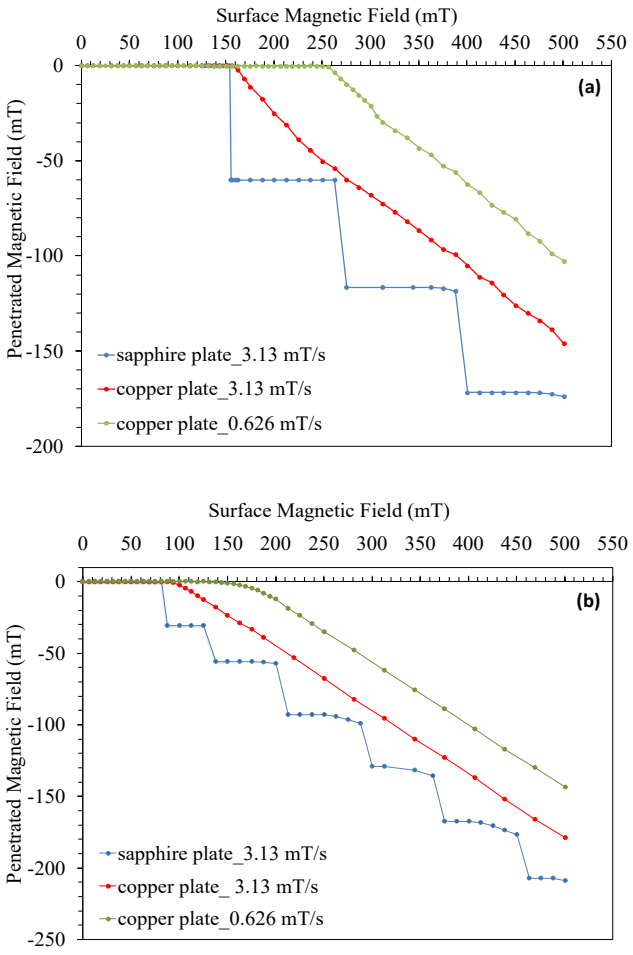

FIG. 12. Full flux penetration measured at 4.35 K from the center Hall probe on (a) 1.5 μm thick Nb_3Sn thin film grown on Al_2O_3 wafer by multilayer sequential sputtering at room temperature and annealed at 950 ^oC by Nizam Sayeed at Jefferson Lab[42]. (b) Nb_3Sn/Al_2O_3 multilayer grown on Al_2O_3 wafer by high-temperature confocal sputtering by Chris Sundahl at University of Wisconsin-Madison. This multilayer sample consists of four 125 nm Nb_3Sn layers separated by 6 nm Al_2O_3 interlayers. A 200 nm thick Nb film was deposited on the back side of the wafers to prevent leakage of RF field during cavity measurements[16]. Flux jumps were observed at a magnet ramp rate of 3.13 mT/s (blue curve). They disappeared when the sapphire separator plate is replaced by a copper plate (red curve). The field onset of flux penetration increased at slower ramp rate 0.626 mT/s (green curve).

each step on FIG 12. comes from a flux micro-avalanche originating at a surface defect. Similar local avalanches were observed in computer simulations of dendtritic flux penetration in superconducting films[43,44]. Such partial flux jumps are more pronounced in Nb_3Sn as compared to Nb and Pb because of much lower electrical and thermal conductivities of Nb_3Sn.

In superconducting thin films thermo-magnetic instabilities result in propagation of fast dendritic flux avalanches[43–45], the field onset of these partial flux jumps decreasing as the magnetic ramp rate increases [35]. These thermomagnetic avalanches can be mitigated by reducing vortex dissipation and improving heat transfer from the sample, particularly by covering a superconducting film with a normal metallic film with high thermal and electric conductivities [45]. The flux jump mitigating measures in our setup were implemented by replacing the sapphire separator plate with a copper plate to improve the efficiency of heat transfer from the sample [37]. As a result, the field jumps detected by the Hall probes disappear at a lower magnet ramp rate, as shown by the red curve in FIG.12. Moreover, the field of full flux penetration increases as the ramp rate decreases as shown by the green curve, the observed B_p being well above B_{c1} in Nb_3Sn. The reduction of B_p by flux jumps can be particularly pronounced in such promising SRF materials as Nb_3Sn and superconducting pnictides which have 2-3 order of magnitude lower thermal and electrical conductivities than Nb.

Investigation of the effect of ramp rate on the flux penetration field is important because it can reveal the relevance of partial flux jumps to the SRF breakdown in accelerator cavities, where the ramp rates of the rf field reaches $\sim 10^9$ T/s. In this case even a few vortex semi-loops penetrating at the surface defect can generate enough heat to ignite propagation of dendritic flux avalanche into the cavity wall. These effects are most pronounced in low conductive SRF materials like Nb_3Sn, which may contribute to the reduced breakdown field observed on Nb cavities coated with Nb_3Sn films as compared to the best Nb cavities [46]. Vortex avalanches can be mitigated by SIS multilayers blocking the propagation of vortex loops in the cavity wall. In that regard, the system described in this work can be useful to investigate the effect of the ramp rate on the penetration field and the ways B_p can be increased by optimizing the film or multilayer geometry and improving heat transfer from local vortex hotspots. For Nb_3Sn thin films and Nb_3Sn/Al_2O_3 multilayers grown on sapphire substrates, we observed an increase of the field onset of flux penetration as the ramp rate decreases. We are planning to coat bulk Nb with SIS multilayers to achieve higher breakdown field using our measurement system at a slower ramp rate to probe the superheating field of the material.

V. CONCLUSION

A Hall probe measurement technique has been developed to detect the field onset of magnetic flux penetration thorough flat samples of SRF materials. Testing the setup on Pb and Nb bulk samples has reproduced the well-known values of critical magnetic fields of these materials. Low conductive thin film materials such as Nb_3Sn films and multilayers exhibit flux jumps due to thermomagnetic flux avalanches. These flux jumps were mitigated by improving heat transfer across the sample and slowing down the magnet ramp rate. This measurement system is now being used to study flux penetration of alternative materials for SRF cavities other than Nb.

ACKNOWLEDGMENTS

We would like to thank Charlie Reece for useful discussion and comments, Gianluigi Ciovati for providing equipment for the measurement system and initial guidance, Nizam Sayeed for Nb_3Sn sample and Chris Sundahl for Nb_3Sn/Al_2O_3 multilayer sample. We also thank the SRF institute and the machine shop staff at the Jefferson Lab for technical support. This work is supported by the National Science Foundation under Grants PHY-1734075 and PHY-1416051, and Department of Energy under Grants DE-SC0010081 and DE-SC0019399.

DATA AVAILABILITY

The data that support the findings of this study are available from the corresponding author upon reasonable request.

[1] H. Padamsee, J. Knobloch, and T. Hays, *RF Superconductivity for Accelerators* (Wiley & Sons, New York, 1998).

[2] H. Padamsee, *RF Superconductivity: Science, Technology, and Applications* (WILEY-VCH Verlag GmbH & Co. KGaA, Weinheim, 2009).

[3] R. Geng, H. Padamsee, A. Seaman, and V. Shemelin, "World record accelerating gradient achieved in a superconducting niobium rf cavity," in *Proc. PAC2005*, Particle Accelerator Conference (JACoW Publishing, Geneva, Switzerland, 2005) pp. 653–655, https://accelconf.web.cern.ch/p05/PAPERS/ROAC009.PDF.

[4] F. Furuta, T. Konomi, K. Saito, G. V. Eremeev, and R. L. Geng, "High gradient results of ICHIRO 9-cell cavity in collaboration with KEK and JLab," in *Proc. SRF2011*, International Conference on RF Superconductivity No. 15 (JACoW Publishing, Geneva, Switzerland, 2011) pp. 386–390, https://accelconf.web.cern.ch/SRF2011/papers/tupo014.pdf.

[5] D. Reschke, S. Aderhold, A. Gössel, J. Iversen, S. Karstensen, D. Kostin, G. Kreps, A. Matheisen, W.-D. Möller, F. Schlander, W. Singer, X. Singer, N. Steinhau-Kühl, A. Sulimov, and K. Twarowski, "Results on large grain nine-cell cavities at DESY: gradients up to 45 MV/m after electropolishing," in *Proc. SRF2011*, International Conference on RF Superconductivity No. 15 (JACoW Publishing, Geneva, Switzerland, 2011) pp. 490–494, https://accelconf.web.cern.ch/SRF2011/papers/tupo046.pdf.

[6] A. Grassellino, A. Romanenko, Y. Trenikhina, M. Checchin, M. Martinello, O. S. Melnychuk, S. Chandrasekaran, D. A. Sergatskov, S. Posen, A. C. Crawford, S. Aderhold, and D. Bice, "Unprecedented quality factors at accelerating gradients up to 45 MVm^{-1}in niobium superconducting resonators via low temperature nitrogen infusion," Supercond. Sci. Technol. **30**, 094004 (2017), https://doi.org/10.1088/1361-6668/aa7afe.

[7] J. Matricon and D. Saint-James, "Superheating fields in superconductors," Phys. Lett. A **24**, 241 (1967).

[8] M. K. Transtrum, G. Catelani, and J. P. Sethna, "Superheating field of superconductors within Ginzburg-Landau theory," Phys. Rev. B **83**, 094505 (2011), https://link.aps.org/doi/10.1103/PhysRevB.83.094505.

[9] F. Pei-Jen Lin and A. Gurevich, "Effect of impurities on the superheating field of type-II superconductors," Phys. Rev. B **85**, 054513 (2012), https://link.aps.org/doi/10.1103/PhysRevB.85.054513.

[10] V.V.Schmidt, *The Physics of Superconductors* (Springer, New York, USA, 1982).

[11] M. Tinkham, *Introduction to Superconductivity* (New York: McGraw-Hill, 1975).

[12] T. L. Hylton and M. R. Beasley, "Effect of grain boundaries on magnetic field penetration in polycrystalline superconductors," Phys. Rev. B **39**, 9042–9048 (1989), https://link.aps.org/doi/10.1103/PhysRevB.39.9042.

[13] J. Durrell, C.-B. Eom, A. Gurevich, E. Hellstrom, C. Tarantini, A. Yamamoto, and D. Larbalestier, "The behavior of grain boundaries in the Fe-based superconductors," Rep. Prog. Phys. **74**, 124511 (2011), https://doi.org/10.1088/0034-4885/74/12/124511.

[14] A. Gurevich, "Enhancement of rf breakdown field of superconductors by multi-layer coating," Appl. Phys. Lett. **88**, 012511 (2006), https://doi.org/10.1063/1.2162264.

[15] A. Gurevich, "Maximum screening fields of superconducting multilayer structures," AIP Advances **5**, 017112 (2015), https://doi.org/10.1063/1.4905711.

[16] C. Sundahl, J. Makita, P. B. Welander, Y.-F. Su, F. Kametani, L. Xie, H. Zhang, L. Li, A. Gurevich, and C.-B. Eom, "Development and characterization of Nb_3Sn/Al_2O_3 superconducting multilayers for particle accelerators," Sci Rep **11**, 7770 (2021), https://doi.org/10.1038/s41598-021-87119-9.

[17] T. Tan, M.A.Wolak, X.X.Xi, T.Tajima, and L. Civale, "Magnesium diboride coated bulk niobium: a new approach to higher acceleration gradient," Sci Rep **6**, 35879 (2016), https://doi.org/10.1038/srep35879.

[18] R. Ito, T. Nagata, H. Hayano, T. Kubo, T. Saeki, Y. Iwashita, R. Katayama, H. Ito, and H. Oikawa, "Development of Coating Technique for Superconducting Multilayered Structure," in *Proc. IPAC2018*, International Particle Accelerator Conference No. 9 (JACoW Publishing, Geneva, Switzerland, 2018) pp. 4954–4956, https://doi.org/10.18429/JACoW-IPAC2018-THPML120.

[19] C. Z. Antoine, M. Aburas, A. Four, F. Weiss, Y. Iwashita, H. Hayano, S. Kato, T. Kubo, and T. Saeki, "Optimization of tailored multilayer superconductors for RF application and protection against premature vortex penetration," Supercond. Sci. Technol. **32**, 085005 (2019), https://doi.org/10.1088/1361-6668/ab1bf1.

[20] A. M. Valente-Feliciano, G. Eremeev, H. L. Phillips, C. E. Reece, J. Spradlin, Q. Yang, D. Batchelor, and R. Lukaszew, "NbTiN based SIS multilayer structures for SRF applications," in *Proc. SRF2013*, International Conference on RF Superconductivity No. 16 (JACoW Publishing, Geneva, Switzerland, 2013) https://accelconf.web.cern.ch/SRF2013/papers/tup088.pdf.

[21] A. Gurevich, "Theory of rf superconductivity for resonant cavities," Supercond. Sci. Technol. **30**, 034004 (2017), https://doi.org/10.1088/1361-6668/30/3/034004.

[22] E. H. Brandt, "The flux-line lattice in superconductors," Rep. Prog. Phys. **58**, 1465 (1995), https://doi.org/10.1088/0034-4885/58/11/003.

[23] E. Zeldov, A. I. Larkin, V. B. Geshkenbein, M. Konczykowski, D. Majer, B. Khaykovich, V. M. Vinokur, and H. Shtrikman, "Geometrical barriers in high-temperature superconductors," Phys. Rev Lett. **73**, 1428–1431 (1994), https://link.aps.org/doi/10.1103/PhysRevLett.73.1428.

[24] E. H. Brandt, "Geometric barrier and current string in type-II superconductors obtained from continuum electrodynamics," Phys. Rev. B **59**, 3369–3372 (1999), https://link.aps.org/doi/10.1103/PhysRevB.59.3369.

[25] T. Junginger, W. Weingarten, and C. Welsch, "Extension of the measurement capabilities of the quadrupole resonator," Rev. Sci. Instrum. **83**, 063902 (2012), https://doi.org/10.1063/1.4725521.

[26] S. Keckert, R. Kleindienst, O. Kugeler, D. Tikhonov, and J. Knobloch, "Characterizing materials for superconducting radioifrequency applications-a comprehensive overview of the quadrupole resonator design and measurement capabilities," Rev. Sci. Instrum. **92**, 064710 (2021), https://doi.org/10.1063/5.0046971.

[27] O. Malyshev, L. Gurran, R. Valizadeh, S. Pattalwar, N. Pattalwar, K. Dumbell, and A. Gurevich, "First Results of Magnetic Field Penetration Measurements on Multilayer S-I-S Structures," in *Proc. IPAC2016*, International Particle Accelerator Conference No. 7 (JACoW, Geneva, Switzerland, 2016) pp. 2245–2247, http://jacow.org/ipac2016/papers/wepmb057.pdf.

[28] A. T. Fiory and A. F. Hebard, "Penetration depths of high Tc films measured by two-coil mutual inductances," Appl. Phys. Lett. **52**, 2165 (1988), https://doi.org/10.1063/1.99757.

[29] D. G. Xenikos and T. R. Lemberger, "Ac susceptibility apparatus for measuring the transition temperature of high-Tc crystals, sintered samples, and films," Rev. Sci. Instrum. **60**, 831 (1989), https://doi.org/10.1063/1.1140330.

[30] J. H. Claassen, M. E. Reeves, and R. J. Soulen Jr., "A contactless method for measurement of the critical current density and critical temperature of superconducting films," Rev. Sci. Instrum. **62**, 996 (1991), https://doi.org/10.1063/1.1141991.

[31] S. J. Turneaure, A. A. Pesetski, and T. R. Lemberger, "Numerical modeling and experimental considerations for a two-coil apparatus to measure the complex conductivity of superconducting films," J. Appl. Phys. **83**, 4334 (1998), https://doi.org/10.1063/1.367193.

[32] T. R. Lemberger and A. Ahmed, "Upper limit of metastability of the vortex-free state of a two-dimensional superconductor in

a nonuniform magnetic field," Phys. Rev. B **87**, 214505 (2013), https://link.aps.org/doi/10.1103/PhysRevB.87.214505.

[33]J. Draskovic, T. Lemberger, B. Peters, F. Yang, J. Ku, A. Bezryadin, and S. Wang, "Measuring the superconducting coherence length in thin films using a two-coil experiment," Phys. Rev. B **88**, 134516 (2013), https://link.aps.org/doi/10.1103/PhysRevB.88.134516.

[34]D. Turner, O. B. Malyshev, G. Burt, T. Junginger, L. Gurran, K. D. Dumbell, A. J. May, N. Pattalwar, and S. M. Pattalwar, "Facility for the characterization of planar multilayer thin film superconductors," Journal of Physics: Conference Series **1559**, 012067 (2020), https://doi.org/10.1088/1742-6596/1559/1/012067.

[35]R. G. Mints and A. L. Rakhmanov, "Critical state stability in type-II superconductors and superconducting-normal-metal composites," Rev. Mod. Phys. **53**, 551–592 (1981), https://link.aps.org/doi/10.1103/RevModPhys.53.551.

[36]E. Altshuler and T. H. Johansen, "Experiments in vortex avalanches," Rev. Mod. Phys. **76**, 471–487 (2004), https://link.aps.org/doi/10.1103/RevModPhys.76.471.

[37]I. H. Senevirathne, J. R. Delayen, A. Gurevich, and A.-M. Valente-Feliciano, "Measurements of Magnetic Field Penetration in Superconducting Materials for SRF Cavities," in *Proc. IPAC'21*, International Particle Accelerator Conference No. 12 (JACoW Publishing, Geneva, Switzerland, 2021) pp. 1208–1211, https://doi.org/10.18429/JACoW-IPAC2021-MOPAB396.

[38]G. Chanin and J. P. Torre, "Critical-field curve of superconducting lead," Phys. Rev. B **5**, 4357–4364 (1972), https://link.aps.org/doi/10.1103/PhysRevB.5.4357.

[39]D. K. Finnemore, T. F. Stromberg, and C. A. Swenson, "Superconducting properties of high-purity niobium," Phys. Rev. **149**, 231–243 (1966), https://link.aps.org/doi/10.1103/PhysRev.149.231.

[40]J. R. Clem, "Theory of ac losses in type-II superconductors with a field-dependent surface barrier," J. Appl. Phys. **50**, 3518–3530 (1979), https://doi.org/10.1063/1.326349.

[41]A. S. Dhavale, P. Dhakal, A. A. Polyanskii, and G. Ciovati, "Flux pinning characterization in cylindrical niobium samples used for superconducting radio frequency cavity fabrication," Supercond. Sci. Technol. **25**, 065014 (2012), https://doi.org/10.1088/0953-2048/25/6/065014.

[42]M. N. Sayeed, H. Elsayed-Ali, M. Burton, G. Eremeev, C. Reece, A.-M. Valente-Feliciano, and U. Pudasaini, "Deposition of Nb_3Sn films by multilayer sequential sputtering for srf cavity application," in *Proc. SRF2019*, International Conference on RF Superconductivity No. 19 (JACoW Publishing, Geneva, Switzerland, 2019) pp. 639–643, https://doi.org/10.18429/JACoW-SRF2019-TUP079.

[43]I. S. Aranson, A. Gurevich, M. S. Welling, R. J. Wijngaarden, V. K. Vlasko-Vlasov, V. M. Vinokur, and U. Welp, "Dendritic flux avalanches and nonlocal electrodynamics in thin superconducting films," Phys. Rev. Lett. **94**, 037002 (2005), https://link.aps.org/doi/10.1103/PhysRevLett.94.037002.

[44]J. I. Vestgården, D. V. Shantsev, Y. M. Galperin, and T. H. Johansen, "Dynamics and morphology of dendritic flux avalanches in superconducting films," Phys. Rev. B **84**, 054537 (2011), https://link.aps.org/doi/10.1103/PhysRevB.84.054537.

[45]P. Mikheenko, A. J. Qviller, J. I. Vestgården, S. Chaudhuri, I. J. Maasilta, Y. M. Galperin, and T. H. Johansen, "Nanosecond voltage pulses from dendritic flux avalanches in superconducting NbN films," Appl. Phys. Lett. **102**, 022601 (2013), https://doi.org/10.1063/1.4775693.

[46]S. Posen, J. Lee, D. N. Seidman, A. Romanenko, B. Tennis, O. S. Melnychuk, and D. A. Sergatskov, "Advances in Nb_3Sn superconducting radiofrequency cavities towards first practical accelerator applications," Supercond. Sci. Technol. **34**, 025007 (2021), https://doi.org/10.1088/1361-6668/abc7f7.